Draft version March 10, 2024
Preprint typeset using LaTeX style AASTeX6 v. 1.0

arXiv:1810.08472v2 [astro-ph.GA] 17 Jan 2019

THE RADIAL ACCELERATION RELATION (RAR): THE CRUCIAL CASES OF DWARF DISCS AND OF LOW SURFACE BRIGHTNESS GALAXIES

C. Di Paolo[1], P. Salucci[1, 2], and J. P. Fontaine[3]

[1]SISSA/ISAS, Via Bonomea 265, 34136 Trieste, Italy
[2]INFN, Sezione di Trieste, Via Valerio 2, 34127 Trieste, Italy
[3]GSSI, Viale Francesco Crispi 7, 67100 L'Aquila, Italy

ABSTRACT

McGaugh et al. (2016) have found, in a large sample of disc systems, a tight nonlinear relationship between the total radial accelerations g and their components g_b arisen from the distribution of the baryonic matter (McGaugh et al. 2016). Here, we investigate the existence of such relation in Dwarf Disc Spirals and Low Surface Brightness galaxies on the basis of Karukes & Salucci (2017) and Di Paolo & Salucci (2018). We have accurate mass profiles for 36 Dwarf Disc Spirals and 72 LSB galaxies. These galaxies have accelerations that cover the McGaugh range but also reach out to one order of magnitude below the smallest accelerations present in McGaugh et al. (2016) and span different Hubble Types. We found, in our samples, that the g vs g_b relation has a very different profile and also other intrinsic novel properties, among those, the dependence on a second variable: the galactic radius, normalised to the optical radius R_{opt}, at which the two accelerations are measured. We show that the new far than trivial g vs $(g_b, r/R_{opt})$ relationship is nothing else than a direct consequence of the complex, but coordinated mass distributions of the baryons and the dark matter (DM) in disc systems. Our analysis shows that the McGaugh et al. (2016) relation is a limiting case of a new universal relation that can be very well framed in the standard "DM halo in the Newtonian Gravity" paradigm.

Keywords: Galaxies, kinematics and dynamics, structure, fundamental parameters, dark matter.

1. INTRODUCTION

A recent study (McGaugh et al. 2016), hereafter referred to as McG+16, claims an empirical discovery that would challenge the idea of dark matter halos surrounding galaxies, or, at least, it would revolutionise our knowledge about the nature of the huge mass discrepancy therein. The standard paradigm relies on collisionless non luminous particles constituting about 25% of the mass energy of the Universe and playing a crucial role on the birth and the evolution of its structures.

The relation, in rotating systems, between the galaxy gravitational potential Φ_{tot} and the radial acceleration $g(r)$ of a point mass at distance r is

$$g(r) = \frac{V^2(r)}{r} = \left| -\frac{d\,\Phi_{tot}(r)}{d\,r} \right| \quad , \tag{1}$$

with $V(r)$ the circular velocity. The baryonic component of the radial acceleration is given by:

$$g_b(r) = \frac{V_b^2(r)}{r} = \left| -\frac{d\,\Phi_b(r)}{d\,r} \right| \quad , \tag{2}$$

where

$$V_b^2(r) = V_d^2(r) + V_{HI}^2(r) + V_{bu}^2(r) \tag{3}$$

is the baryonic contribution to the circular velocity. In Eq. 3, the velocities $V_i = |-r\,d\Phi_i(r)/dr|^{1/2}$ are the solutions of the separated Poisson equations: $\nabla^2\Phi_i(r) = 4\pi G\rho_i$. ρ_i is equal to the stellar disc, the HI disc and the bulge mass

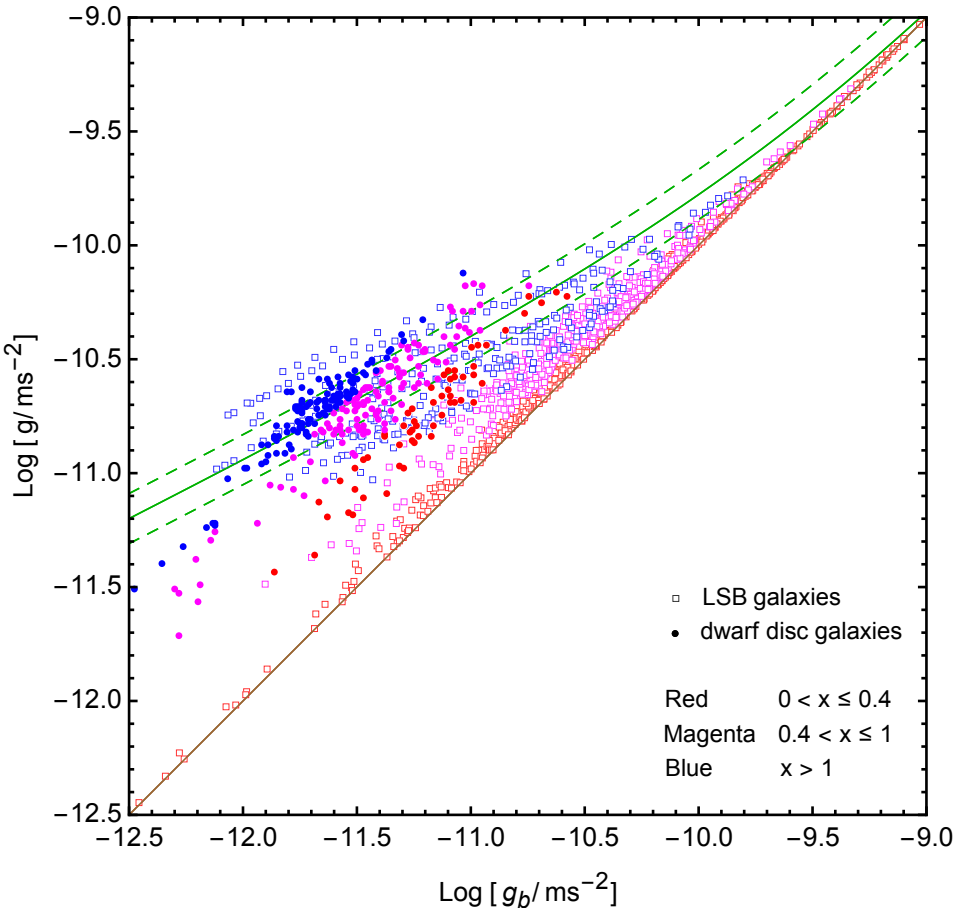


Figure 1. Relationship between the total acceleration g and its baryonic component g_b. $x = r/R_{opt}$. *Red*, *magenta* and *blue points* correspond to radial bins with increasing distance from the galactic center (see *legend*). Also shown: the McGaugh et al. (2016) relationship (*solid green line*) with its $1\,\sigma$ errorbars of 0.11 dex (*dashed green lines*); the Newtonian relationship $Log\, g = Log\, g_b$ (*brown line*). See also Fig. 6 in Appendix A, for LSBs data with very low values of $Log\, g$ and $Log\, g_b$.

densities and Φ_i are the gravitational potentials of the i-components. Obviously we have:

$$g_h(r) = g(r) - g_b(r) \quad , \tag{4}$$

where g_h refers to the dark matter contribution to the radial acceleration g.
McG+16 investigated 153 galaxies across a wide range of Hubble types and luminosities with new high-quality data from the Spitzer Photometry and Accurate Rotation Curves (SPARC) database. The analysis includes (see Lelli et al. (2016) for details):

i) near-infrared ($3.6\mu m$) observations that trace the distribution of stellar masses under the assumption of 0.5 $M_\odot/L_\odot$ for the value of the stellar mass to light ratio in this band;

ii) the 21 cm observations that trace the distribution of the atomic gas and the velocity fields.

They found that the radial acceleration $g(r)$ shows an anomalous feature: it correlates at any radius and in any object, with its component generated from the baryonic matter $g_b(r)$ in a way that it is :

i) very different from the $g = g_b$ relationship expected in the Newtonian case with the presence of the only baryonic matter;

ii) claimed of difficult understanding in the standard Newtonian + dark matter halos scenario.

In detail, the McGaugh relationship (see Fig 1 and Fig 3 in McG+16) relies on 153 objects for a number of 2693

independent circular velocity measurements. Each of them yields the pairs (g_b, g), well fitted by:

$$Log\, g(r) = Log \left(\frac{g_b(r)}{1 - exp\left(-\sqrt{\frac{g_b(r)}{\tilde{g}}}\right)} \right) \quad , \tag{5}$$

with $\tilde{g} = 1.2 \times 10^{-10}\, ms^{-2}$. At high accelerations, $g \gg \tilde{g}$, Eq. 5 converges to the Newtonian relation $g = g_b$; while, at lower accelerations, $g < \tilde{g}$, Eq. 5 strongly deviates from the latter (McGaugh et al. 2016; Li et al. 2018).

A recent investigation of the McG+16 relationship has been performed by Salucci (2018a,b) (hereafter S18) in three very large samples of *normal spirals* by exploiting three specifically devised methods of deriving g_h (as shown in Eq. 4). In these works, the stellar mass distribution is estimated kinematically, by means of the mass modelling of the rotation curves, rather than being estimated from spectrophotomery as in McG+16. The outcome is a $g(g_b)$ relationship, with a r.m.s. of 0.15 dex and with a quite small systematical difference of 0.2 dex from Eq. 5 (Salucci 2018b). These results, totally framed in the DM scenario and obtained by means of novel methods of mass modelling, confirm the McG+16 relationship in normal Spirals.

Recently, Karukes & Salucci (2017) and Di Paolo & Salucci (2018) have obtained the radial distribution of the total, baryonic and dark matter for 36 dwarf spirals, yielding 315 acceleration measurements, and 72 Low Surface Brightness (LSB) galaxies, yielding 1601 acceleration measurements (see also Appendix A for further details). These accelerations occupy a region in the $g - g_b$ plane (see Fig. 1) compatible with that covered by previous works, but that, in addition:

a) reaches smaller values along the vertical axis, considering our smallest value of $Log\, g/ms^{-2} \simeq -12.5$ (-14.5, see Appendix A) and the McG+16 smallest unbinned value of $Log\, g/ms^{-2} \simeq -11.4$;

b) pertains to different Hubble Types than the bulk of the objects in McG+16; it is worth to specifying that the sample of McG+16 (153 rotating objects) has dwarf and LSB discs alongside with a large number of normal Spirals. In our work, we have only dwarf discs (here called DD) and LSB galaxies.

A very important element of our analysis is the baryonic fraction $f_b(r)$, which varies in galaxies of different dimensions and Hubble Types. It will pivotal to frame our data and those of McG+16 and S18 within the standard "DM halo in the Newtonian Gravity" paradigm. Moreover, we will understand why the McG+16 relation is only a limit of a more complex universal relation.

Let us define the distribution of stars in disc galaxies, by means of their surface brightness, which is almost always given, in disc systems, by $\mu(r) = \mu(0) + 1.086\, r/R_d$ (Freeman 1970), where R_d is the exponential disc scale length ($\mu(0)$ is variable object by object). In this work, the accelerations are in m/s^2 and the distances in kpc. The optical radius R_{opt} is defined as the radius encompassing 83% of the total luminosity; $R_{opt} = 3.2\, R_d$. The optical velocity V_{opt} is the circular velocity measured at R_{opt}. Let us notice that in this paper, we will use alternatively the quantity x and $r/R_{opt} \equiv x$. In addition, our system of coordinates is r, φ, z.

The work is organised as follows: in section 2, we will describe the dwarf discs and LSBs samples; in section 3, we briefly describe the Universal Rotation Curve method used in our analysis; in section 4, we build the g vs g_b relation followed, in section 5, by a 3D analysis that involves the baryonic fraction $f_b(r)$ and the additional variable x. Finally, in section 6 we report the consequences of our results.

2. THE DD AND LSB SAMPLES

The sample of dwarf discs (Karukes & Salucci 2017) that we use in this work is drawn from the Local Volume catalog (Karachentsev et al. 2013). The faintest objects are 3 magnitudes fainter with respect to the sample of spirals of McG+16 and S18. These galaxies explore quite smaller mass scales than the normal Spirals. The criteria adopted to select the objects are described in (Karukes & Salucci 2017). In detail, the sample consists of 36 galaxies (two among them are in common with the LSB sample) whose structural properties span the intervals: $-19.9 \lesssim M_K \lesssim -14.2$, $0.18\, kpc \lesssim R_d \lesssim 1.63\, kpc$, $17\, km/s \lesssim V_{opt} \lesssim 61\, km/s$. All galaxies are bulgeless disc systems in which the rotation, corrected for the pressure support, totally balances the gravitational force.

The sample of LSBs consists of 72 disc galaxies. They are objects which emit an amount of light per area much smaller than normal spirals (de Block 2000; McGaugh 1994; Impey & Bothun 1997) and don't lay on the $L \propto R_d^2$

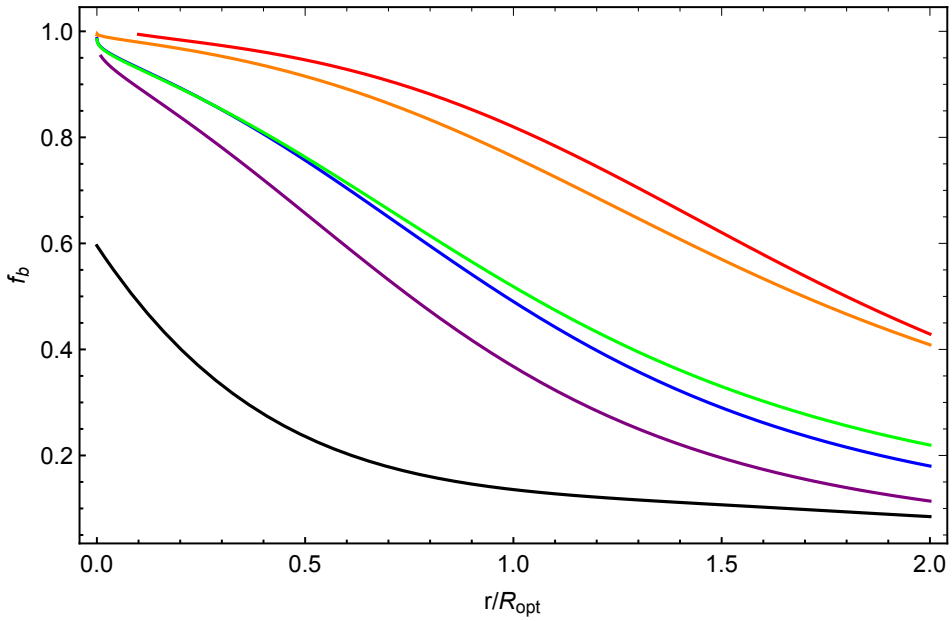


Figure 2. Baryonic fraction as function of r/R_{opt}, derived by the URCs of DD (*black line*, with $\langle V_{opt} \rangle = 40\,km/s$) (Karukes & Salucci 2017) and of LSBs (*purple, blue, green, orange* and *red*, with: $\langle V_{opt} \rangle = 43, 73, 101, 141, 206\,km/s$) (Di Paolo & Salucci 2018). For the uncertainties on the $f_b(x)$ see text and Appendix D.

relationship of the latter. The sample of rotation curves is selected from literature (Erkurt et al. in preparation)[1] and characterised by objects whose optical velocities V_{opt} span from ~ 24 km/s to ~ 300 km/s.

For both DD and LSB samples, the available photometry and kinematics are of sufficient quality to allow us to obtain a proper mass modeling, by means of the technique of the Universal Rotation Curve (URC) (Persic et al. 1996).

3. THE MASS DISTRIBUTION IN DISC SYSTEMS BY EXPLOITING THE URC

The URC compacts the structural properties of rotating systems (Persic et al. 1996; Salucci et al. 2007). As starting point, all galaxies of a given sample are binned in different groups/families according to their V_{opt} (in the case of our samples) and then co-added in terms of $x \equiv r/R_{opt}$, their radial normalised coordinate. Galaxies inside a certain limited range of V_{opt} have, approximately, all the same baryonic and DM distribution, once they are expressed in normalised radial coordinate x. For the present samples, the DD galaxies are grouped in a single bin (Karukes & Salucci 2017) and the LSB galaxies are grouped in five bins (according to their increasing V_{opt}) (Di Paolo & Salucci 2018).

The URC model is based on an exponential disc (Freeman 1970) for the stellar component and the Burkert density profile (Burkert 1995) for the dark matter halo (preferred in discs systems, see (Salucci & Burkert 2000; Karukes & Salucci 2017; de Blok & Bosma 2002)). For the disc component, the Tonini et al. HI disc (Tonini et al. 2006; Evoli et al. 2011) is considered in DD galaxies and a bulge component (Yegorova & Salucci 2007) is taken into account for the largest LSB galaxies (Das 2013) . Let us notice that, for LSBs, the gas contribution to the circular velocity can be considered negligible in view of the aim of this paper. See Appendix C.

We fit with the URC the co-added rotation curves for each of the 1 + 5 families. This provides us with $V_{URC}(r/R_{opt}, V_{opt})$ and $V_{URC,\,b}(r/R_{opt}, V_{opt})$, i.e. the circular velocity and its baryonic component (see Appendix B for further details about the URC method).

The baryonic fraction f_b as function of r/R_{opt} for galaxies tagged by V_{opt} is given by:

$$f_b(r/R_{opt}, V_{opt}) = \frac{V^2_{URC,\,b}(r/R_{opt}, V_{opt})}{V^2_{URC}(r/R_{opt}, V_{opt})} \quad . \tag{6}$$

See Fig. 2. Note that, going from the inner to the external radii and from the biggest to the smallest galaxies, the

[1] In Appendix F we provide the references for the RC data and other galactic properties (see Tab. 1).

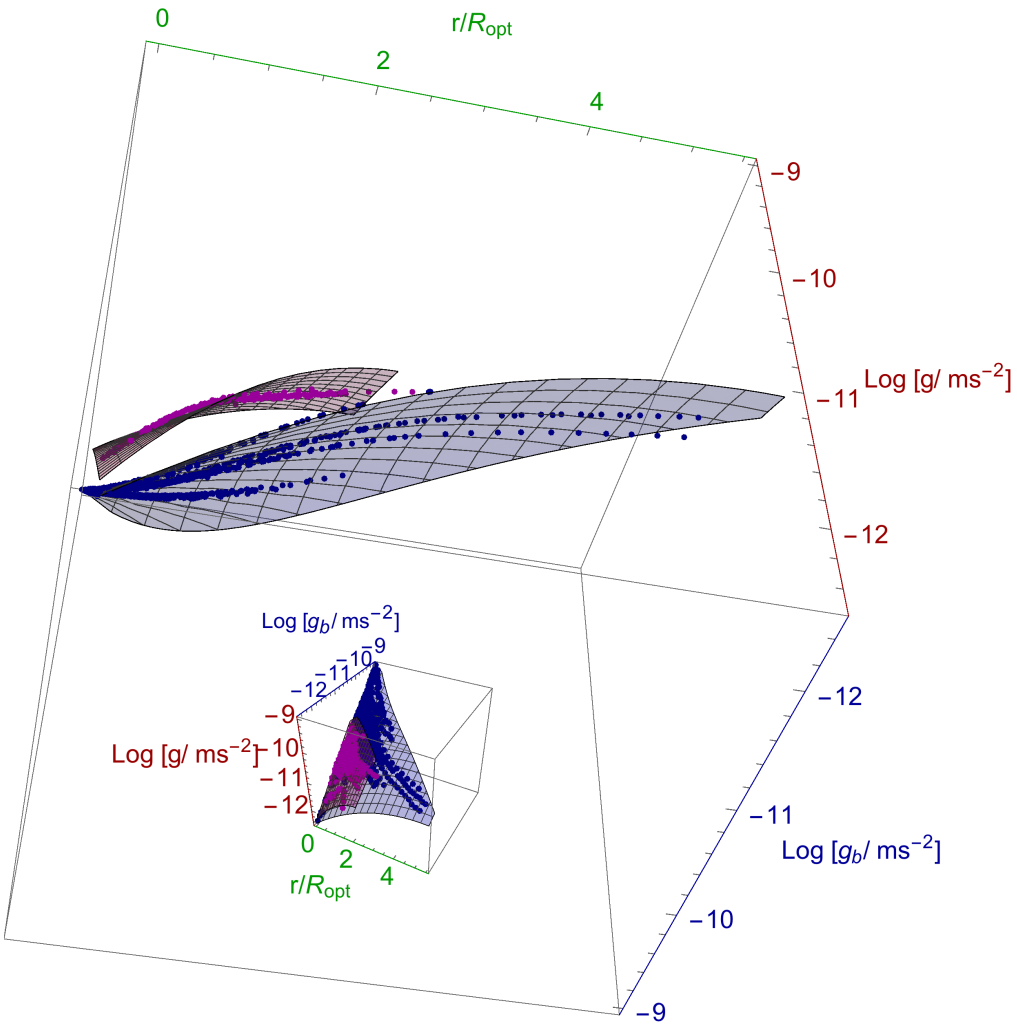


Figure 3. Relation among total acceleration g, baryonic acceleration g_b and normalised radii r/R_{opt}. The *magenta* and *blue points* refer to DD and LSB galaxies data respectively. The *surfaces* are the results from the best fit models.

baryonic component becomes less and less relevant than the DM one. It is remarkable that a very similar behaviour of $f_b(r/R_{opt}, V_{opt})$ is found also in Spirals (Salucci et al. 2007; Lapi et al. 2018).

Eq. 6, recast in other terms, becomes: $V^2_{URC,\,b}(r) = f_b(r, V_{opt}) V^2_{URC}(r)$ and, consequently, with Eq. 1, we have for each galaxy:

$$g_b(r) = f_b(r, V_{opt})\, g(r) \quad . \tag{7}$$

Then, by summarising: in each galaxy with disc scale length $R_{opt}/3.2$, rotation curve $V(r, R_{opt})$ with V_{opt} tag value, we have : $g(r) = V^2(r)/r$ and $g_b(r) = f_b(r) g(r)$, where $f_b(r)$ is the baryonic fraction (hereafter, for semplicity, we drop the family tag V_{opt}). Notice that $g(r)$ is totally observed, $g_b(r)$ has a part derived from the baryonic component to the rotation curves obtained by the baryonic mass distribution.

4. RESULTS

The emerging g vs g_b relationships, obtained for DD and LSB galaxies, are shown in Fig 1. We realise that the universality of the $g(g_b)$ relation, holding in normal spirals (McGaugh et al. 2016; Salucci 2018a) breaks down in our samples. The scatters of DD and LSB data with respect to the McG+16 relation are 0.17 dex and 0.31 dex respectively. This big discrepancy cannot be due to observational or systematical errors, in fact we have used high-quality rotation

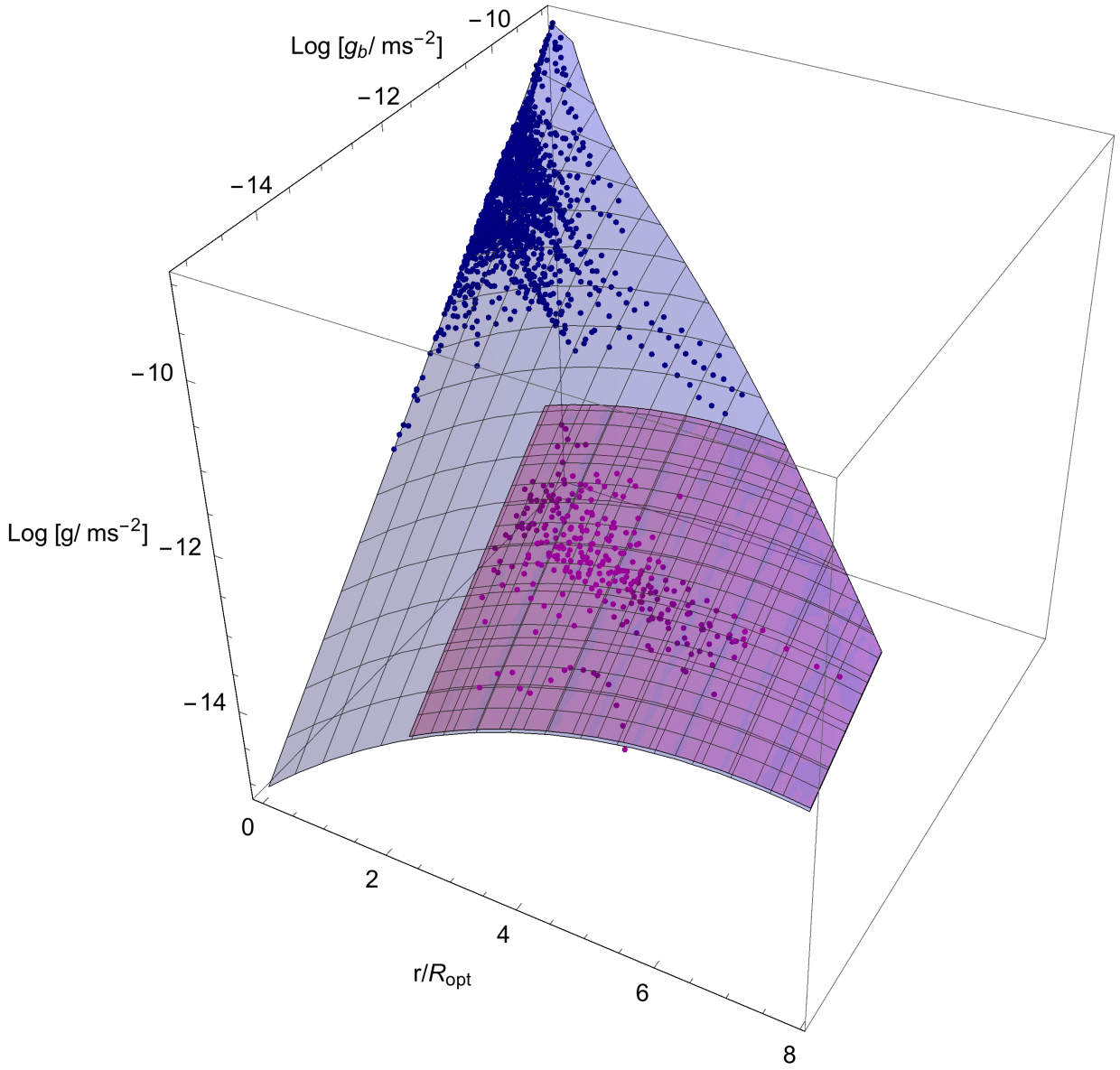


Figure 4. The relationships among the total acceleration g, the baryonic acceleration g_b and the normalised radii r/R_{opt} for our two samples. The *magenta* and *blue points* refer to DD and LSB data, alongside with their best-fit *surfaces*. The LSBs measurements extend in the $Log\, g/ms^{-2}$ and $Log\, g_b/ms^{-2}$ range $\sim [-12.5\,,\,-9.0]$. The fitting surface well represent also the very low accelerations data discussed in the Appendix A.

curves, so that the observational uncertainties on $V^2(r)$, leading to $g(r)$, are are less than 20%. Systematical errors are present only on the quantities $g_b = f_b g$, due to f_b. From the modelling of the co-added rotation curves in Spirals, DD and LSBs, the quantity f_b has fitting uncertainties running from 10% at higher luminosity to 30% at lower luminosity. This implies that the uncertainties on $Log\, g_b$ lay in the range between 0.13 dex and at most 0.19 dex. In this work, as those discussed in previous sections, the determination of g and g_b is not an issue. It is important to note in Fig. 1 that there are many points strongly discrepant with respect to the McG+16 relation along *both* axes: in detail 1 dex on the $Log\, g_b$ axis and the same value on the $Log\, g$ axis, where our measurements can be considered almost error-free.

Let us stress that, as consequence of the method employed to derive g_b, we cannot have: $g_b > g$; only when we consider the fitting uncertainties on g_b, we obtain that this quantity can (sligthly) overcome g in average by a value of ~ 0.1 dex at 2σ level of uncertainty (see Appendix D). This point is irrelevant for the scope of this paper.

The data relative to the inner regions of galaxies (red data) are the closest to the equality line $Log\, g = Log\, g_b$, while data relative to more external regions (blue data) of galaxies tend to depart from the equality line towards the region

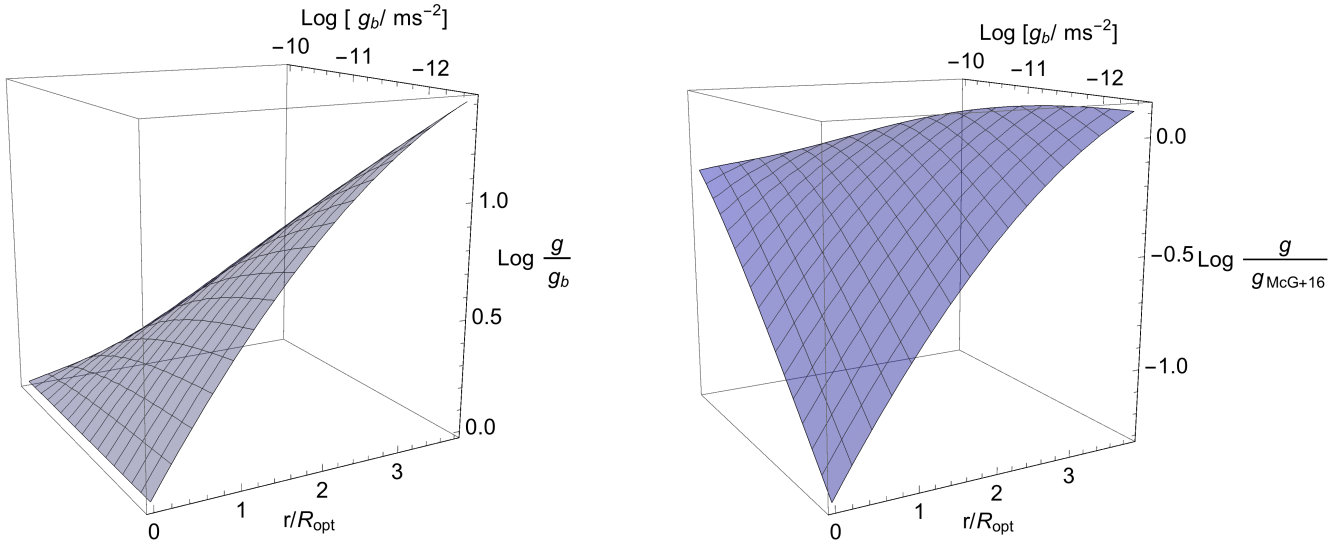


Figure 5. The *surface in left panel* is given by the difference between the LSBs $GGBX$ relationship (Eq. 8) and the Newtonian value $Log\, g_b$. The *surface in right panel* is given by the difference between the LSBs $GGBX$ relationship and the McG+16 relation (Eq. 5).

covered by McG+16 relation and then go beyond, with $Log\, g > Log\, g_b$. This behaviour is intrinsically related to the mass distribution in galaxies: the higher is the baryonic fraction f_b, the more g is close to g_b, and reversely the lower is f_b, the more g overcomes g_b.

5. THE UNIVERSALITY OF THE $GGBX$ RELATIONSHIP

It is evident that, in both DD and LSB samples, pairs of accelerations (g , g_b) residing at different radii r/R_{opt} don't overlap. We realise that a relationship between g and g_b necessarily must involve also the position x, where the two accelerations are measured, and the Hubble type of the objects. This is shown in our new 3D relationship, Eq. 8, (hereafter $GGBX$ relation) among the $Log\, g - Log\, g_b - x$ quantities. Starting from the McG+16 relation (in order to have a straightforward comparison), we added new terms to find the best fitting model for LSB data. The best and simplest model that we found is:

$$Log\, g_{_{LSB}}(x,\, Log\, g_b) = (1 + a\, x)\, Log\, g_b + b\, x\, Log\, [1 - exp(-\sqrt{g_b(x)/\tilde{g}})] + c\, x + d\, x^2 \quad , \tag{8}$$

where the fitting parameters a, b, c, d assume the best-fit values -0.95, 1.79, -9.01, -0.05 respectively. The scatter of LSB data from the fitting surface is considerably reduced, down to 0.05 dex, i.e. to a sixth of the scatter from the McG+16 relation. Let us notice that the model used in Eq. 8 is just an empirical function used to fit the data that recovers $Log\, g \to Log\, g_b$ when $x \to 0$. Then the number of free parameters of the x part in the above relation expresses only our ignorance of the actual functional form of the relationship and not the fact that the $g(g_b, x)$ surface is not smooth and of negligible thickness.

In the case of DD galaxies, by simply applying translations and/or dilatations to Eq. 8 along the three involved axes, we obtain the following best fitting model:

$$Log\, g_{_{DD}}(x,\, Log\, g_b) = Log\, g_{_{LSB}}\left(\frac{x}{l} + h,\, \frac{Log\, g_b}{m} + n\right) + q \quad . \tag{9}$$

We found a perfect fit of the data when the fitting parameters l, h, m, n, q assume the best-fit values 0.49, 2.41 , 0.74 , 1.72 , 1.19 respectively. The scatter of DD with respect to the fitting surface is considerably reduced, with a value of 0.03 dex, i.e. about a fifth of the scatter from the McG+16 relation.

We show in Fig. 3 the DD and LSB data in the $g - g_b - x$ space, with their best fitting surfaces from Eq. 8-9. The result is extremely remarkable. It shows a precise relation linking the total and baryonic acceleration, the galactocentric distance $x \equiv r/R_{opt}$ and even the morphology of galaxies. The scatter of both LSB plus DD data (after the translation and dilations given by the parameters l, h, m, n, q; see Fig. 4) from the $GGBX$ surface is only 0.05 dex,

about a sixth of their scatter from the McG+16 relation (0.29 dex); moreover it is also lower then the scatter of 0.13 dex of McG+16 sample from McG+16 relation. The statistical significance is overwhelming, but its physical meaning is not immediate. Let us stress that the data g, g_b, x form, for LSBs and DDs, two very thin *surfaces* that can be overlapped through a simple coordinate transformation. Again, the number of the fitting parameters reflects our ignorance of the analytical representation of the $g(g_b, x)$ relation, not the statistical relevance of the surfaces defined by data.

5.1. *Understanding the GGBX relationship*

Our relationship deviates both from the Newtonian and from the McG+16 relationship. In particular, by considering the LSBs, i.e. our most numerous sample, we observe that:

i) the deviation from the Newtonian relation is more evident at larger galactocentric radii and for smaller g_b values. See the left panel of Fig. 5, which shows the difference $Log\, g_{_{LSB}}(x,\, Log\, g_b) - Log\, g_b$;

ii) the deviation from the McG+16 relation is particularly evident at smaller galactocentric radii and for smaller g_b values. See the right panel of Fig. 5, which shows the difference $Log\, g_{_{LSB}}(x,\, Log\, g_b) - Log\, g_{_{McG+16}}$.

We highlight that these results are related to the mass distribution in galaxies: any $g_b(r)$ corresponds to very different values of $g(r)$ according to the tag velocity V_{opt} (or luminosity), the normalised radius r/R_{opt} and the Hubble Type of the galaxy in question. This is consequence of the fact that $g_b(r) = f_b(r)g(r)$ and that $f_b(r)$, related to the mass distribution in galaxies, depends on the tag velocity V_{opt} (or luminosity), the normalised radius r/R_{opt} and the Hubble Type of the galaxy in question (Fig. 2).

It is worth to show how all the above results, including the disagreements with McG+16, are evident when we plot the GGBX relation in *individual* objects (see Appendix E).

In conclusion, straightforward facts are that:

(i) the same values of the pairs (g, g_b) found in the outer region of big spirals are replicated in the inner region of small spirals, provided that approximately $r \geq R_d$. This explains the genesis of McG+16 and S18 findings;

(ii) given one spiral and one LSB, both with the same V_{opt} and then very similar $f_b(x)$, they can show very different $f_b(r)$ in physical radial units. This happens because LSBs usually have much more extended R_D than spirals (see Fig. 9 in (Di Paolo & Salucci 2018)). Thus, $f_{b,_{LSB}}(r) > f_{b,_{spiral}}(r)$. Then, at fixed value of g_b, very different values of g can correspond, and vice-versa. This mainly explains the failure of the McG+16 relation in LSBs.

6. CONCLUSION

The two accelerations relationship (eq. 5) by McG+16 has attracted a large interest. It is claimed and thought that it provides crucial evidence about the issue of dark matter. In this work, we have investigated the $g_b - g$ relationship (found by McG+16 for a sample dominated by normal spirals), in the recent sample of 36 Dwarf Discs and 72 LSB galaxies, whose optical velocities span from $\sim 17\, km/s$ to $\sim 300\, km/s$, covering the full population of galaxies sizes and luminosities. We analyzed overall 1904 velocity data and modeled them by involving an exponential stellar disc, a Burkert dark matter halo density profile (Karukes & Salucci 2017; de Blok & Bosma 2002) and, in particular, we also considered the Tonini et al HI discs (Tonini et al. 2006) in DD galaxies and a bulge component in larger LSB galaxies (Karukes & Salucci 2017; Di Paolo & Salucci 2018). Then, we have derived the 1904 (g_b, g) pairs in the same way of McG+16 with the difference that the disc masses are obtained kinematically. This difference of methods, however leads to estimates of the disc masses that agree within their uncertainties. The great discrepancy between the McG+16 relationship and ours does not arise from the adopted values of the stellar disc + HI disc masses.

In our objects $Log\, g/ms^{-2}$ lays in the range between -14.5 and -9. On the other hand, the unbinned data $Log\, g/ms^2$ in the McG+16 relationship range between -11.4 and -8. The results of our tests involving the DD and LSBs samples show empirically that the radial acceleration g in galaxies is not simply a universal function dependent on the baryonic acceleration g_b (as claimed by McG+16 in eq. 5), but also depends on the galactic radius expressed in normalised units r/R_{opt}.

The emerging relationship mirrors the properties of the DM in galaxies, whose fraction changes along the galactic radius, becoming more dominant on the baryonic one in the external regions, in a way which depends on the morphology and the luminosity of the galaxy (Fig. 2) (Persic et al. 1996).

For each sample, we have established a universal relation $g = f(g_b, x)$ (that we call $GGBX$ relationship), with x the normalised radius with respect the optical radius R_{opt}. Moreover, we can go from DD relationship to the LSB one by means of translations and/or dilatations of the three involved variables. The individual average scatter around these $GGBX$ new surfaces (created by g, g_b x data) is remarkably reduced with respect to that around to the McG+16 relation, more precisely it becomes a fifth and a sixth for DD and LSB galaxies data, respectively.

Our relationship deviates both from the Newtonian and from the McG+16 2D relationship. In particular, the deviation from the Newtonian relation is more evident at larger galactocentric radii and for smaller g_b values, while the deviation from the McG+16 relation is particularly evident at smaller galactocentric radii and for smaller g_b values.

It is worth saying that the results are intrinsically related to the *mass distribution in galaxies*, i.e. to the variation of the baryonic fraction f_b along the galactocentric radius and on the fact that it changes when we consider galaxies of different luminosity and different Hubble Type. This implies that, when considering different galaxies, a same value of g_b can be found at very different radii r and can correspond to very different values of g. This is the main explanation of the discrepancy among LSBs, DD and Spiral galaxies considered in McG+16 and S18.

In this paper a new relation among the dynamical quantities in disc galaxies has emerged. The further investigation of the origin of such relation and the consequences in single objects will be shown in another next paper in preparation by Di Paolo et al. (2018).

In conclusion, we find that the $GGBX$ relationship (Eq. 8-9) is universal and framed in the DM + Newtonian gravity scenario. We point out that this relation stems out of the properties of $V^2(x)$ and $f_b(x)$. Therefore, it does not pose issues to the ΛCDM + baryonic feedback scenario.

Crucial properties of the DM are instead unlikely to come from the $g - g_b$ relationship, in fact the DM halo density profile is $\rho(r) = 1/(4\pi G r^2)\ \frac{d}{dr}[g(r)r^2(1-f_b(r))]$ and crucially depend on quantities not present in the $g-g_b$ relationship: e.g. $dV(r)/dr$, $V^2(r)\, df_b(r)/dr$. Whether our $GGBX$ compacts all the structural properties of DM halos will be left to a further work (Di Paolo et al. (2018) in prep.).

ACKNOWLEDGMENTS

We thank F. Nesti, A. Lapi, L. Danese and A. Erkurt for useful discussions. We also thank G. Costa for helps that have improved the presentation of the results of this paper.

APPENDIX

A. THE EXTENDED $G - G_B$ PLANE

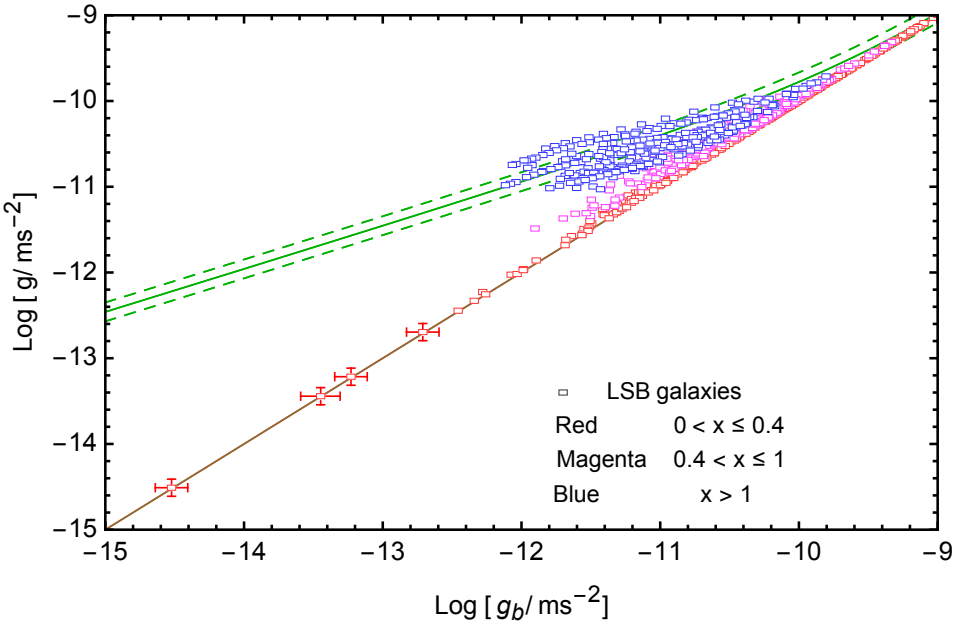


Figure A6:. Relationship between the total acceleration g and its baryonic component g_b, for LSB data. $x = r/R_{opt}$. The figure is analogous to Fig. 1, but also includes data till the lowest values of $Log\, g$ and $Log\, g_b$. The 4 "special points" with very small values of $Log\, g$ - $Log\, g_b$ are shown with their 1σ uncertainties.

For completeness, we show all the LSBs data in Fig. 6, in order to highlight the extension of $Log\, g$ and $Log\, g_b$ values to ~ -14.5 (with the argument expressed in m/s^2). We highlight that, originally, we had 1605 data for the LSB galaxies. 4 "special points" of them have very low values of $Log\, g$ and $Log\, g_b$ laying in the range [-14.5, -12.5]. See Fig.

6. These data strongly support our result shown above, i.e. the discrepancy of LSB accelerations from the McG+16 relationship, however, we keep them separately from the rest of the data because they are too few to cover their wide magnitude range (only 4 points in a range of 2 dex).

B. THE UNIVERSAL ROTATION CURVE (URC) METHOD

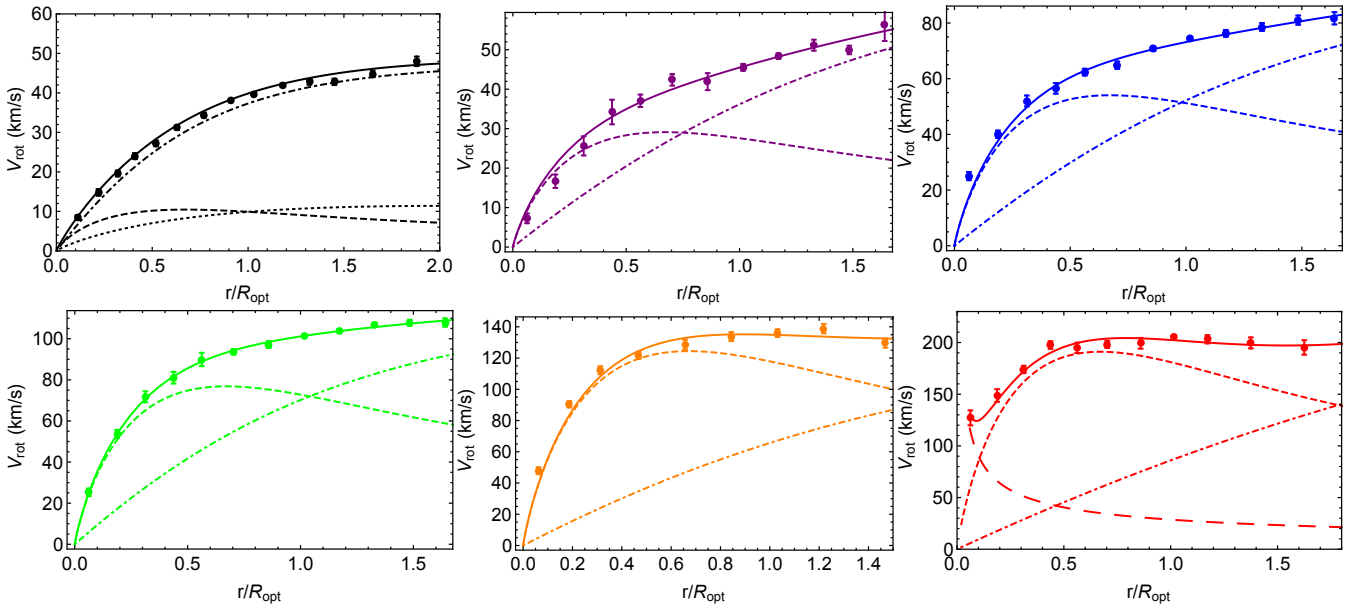


Figure B7:. Best fit URC velocity models of the co-added RCs of the unique velocity bin representative of DD galaxies (*black*, with $\langle V_{opt}\rangle = 40\,km/s$) and of the five velocity bins, representative of the LSBs (*purple, blue, green, orange* and *red* with: $\langle V_{opt}\rangle = 43,\ 73,\ 101,\ 141,\ 206\,km/s$). The *dashed, dotted, dot-dashed, long-dashed* and *solid lines* are the stellar disc, HI disc, dark matter, bulge and total contributions to the circular velocities, respectively.

The URC is derived, firstly, by luminosity/optical velocity and normalized radial binning of a large number of individual rotation curves that yield suitable co-added rotation curves $V_{co-add}(x^2, \lambda^3)$, see for details (Persic et al. 1996; Salucci et al. 2007). For the present work: the DD galaxies are grouped in a single family (Karukes & Salucci 2017), the LSB galaxies are grouped in five families, each with increasing tag average velocity $\langle V_{opt}\rangle$.

The co-added curves (RCs) are very well reproduced by a suitable analytical velocity model that we call $V_{URC}(x, \lambda)$ (see (Karukes & Salucci 2017; Di Paolo & Salucci 2018)). [4]

The URC method has been applied, so far, to Spirals, LSB and dwarf discs. It consists in the sum in quadrature of four terms, $V_{d,URC}$, $V_{HI,URC}$, $V_{bu,URC}$, $V_{h,URC}$, each of them describing the contribution from the stellar disc, the HI gaseous disc, the central bulge and the dark halo. Then:

$$V^2_{co-added}(x,\lambda) \simeq V^2_{URC}(x,\lambda) = V^2_{d,URC}(x,\lambda) + V^2_{HI,URC}(x,\lambda) + V^2_{bu,URC}(x,\lambda) + V^2_{h,URC}(x,\lambda) \quad , \tag{B1}$$

where the l.h.s. are the co-added RCs and the r.h.s is the analytical model with which we fit the former.

For simplicity, hereafter we drop the tag "URC" in the model velocity components.

$V_{URC}(x, \lambda)$ fits extremely well all $V_{co-added}(x, \lambda)$ (see Fig. 7) of spirals (Persic & Salucci 1991; Salucci et al. 2007; Persic et al. 1996), DD (Karukes & Salucci 2017) and LSB (Di Paolo & Salucci 2018), and provides us with an accurate analytical representation of the individual rotation curves.

The stellar component is described by means of the well-known exponential disc (Freeman 1970) with surface density profile $\Sigma_D(r) = \frac{M_d}{2\pi R_d^2}\, exp(-r/R_d)$.

Caveat the distance of the galaxy, the gas contribution is known from observations (e.g. see (Evoli et al. 2011)). This component is described as it follows: the total mass is obtained from the 21-cm flux and its radial distribution is

[2] $x = r/R_{opt}$
[3] λ is equal to M_k or V_{opt}, (i.e. λ is the galaxies family identifier).
[4] For our objects we know the values of their R_d, so that we can express the URCs in term of their physical radial units $V_{URC}(r)$.

given by $\Sigma_{HI}(r) = \frac{M_{HI}}{2\pi(3\,R_d)^2}\,exp(-r/3\,R_d)$ (Tonini et al. 2006; Evoli et al. 2011; Wang et al. 2014). Then:

$$V_d^2(r) = \frac{1}{2}\frac{G\,M_d}{R_d}(3.2\,r/R_{opt})^2(I_0K_0 - I_1K_1)\ ; \qquad V_{HI}^2(r) = \frac{1}{2}\frac{GM_{HI}}{3R_D}(1.1\,r/R_{opt})^2(I_0K_0 - I_1K_1) \tag{B2}$$

where M_d is the stellar disc mass, M_{HI} is the gaseous disc mass (correcting by a factor 1.3 in order to account for the He abundance), I_n and K_n are the modified Bessel functions computed at $1.6\,x$ and $0.53\,x$ for the stellar and the gaseous disc respectively.

Let us notice that, in LSBs, the gas contribution to the circular velocity is negligible for the scope of this paper (see also Appendix C).

In the largest velocity bin of LSBs, in the URC model we have included a bulge component by adopting:

$$V_{bu}^2(r) = \alpha_b V_{in}^2(r/r_{in})^{-1} \quad , \tag{B3}$$

where V_{in} and r_{in} are values referred to the innermost circular velocity measurements and α_b is a parameter varying from 0.2 to 1 (see e.g. (Yegorova & Salucci 2007)).

Therefore, for bulgeless DD galaxies we assume, as baryonic contribution, $V_b^2(r) = V_d^2(r) + V_{HI}^2(r)$, while for the LSBs we assume $V_b^2(r) = V_d^2(r)$ for the four galaxies families (velocity bins) characterised by the smallest V_{opt} and $V_b^2(r) = V_d^2(r) + V_{bu}^2(r)$ for galaxies with the largest V_{opt} (Salucci et al. 2000; Das 2013).

For the DM halo velocity contribution we adopt the cored Burkert profile (Burkert 1995):

$$V_h^2(r) = 2\pi G\rho_0\frac{R_0^3}{r}[\ln(1 + r/r_0) - tg^{-1}(r/r_0) + 0.5\ln(1 + (r/r_0)^2)] \tag{B4}$$

where ρ_0 is the central mass density and r_0 is the core radius.

By resuming, the co-added rotation curves $V_{co-added}$ are very well fitted by V_{URC} (see Fig. 7) and the best fitting parameters M_d, α_b, ρ_0, r_0 result all as a function of λ (V_{opt} or M_K). We direct the interested reader to (Karukes & Salucci 2017; Di Paolo & Salucci 2018).

C. THE HI COMPONENT EFFECT ON THE G-G_B PLANE

We have investigated the g - g_b plane by including also the gas component in LSB galaxies when fitting their rotation curves. For these galaxies, we assumed the contribution of the gaseous component by means of the r.h.s. of Eq. B2 and considering the mass M_{HI} as a free parameter (M_{HI} includes HI + He components). The results are: the gas is important only in the first velocity bin; however, the inner regions are quite dominated by the stellar component and the gas component is of limited importance. In Fig. 8, we fit the first LSB co-added rotation curve (velocity bin) without/with the gas contribution. In both cases, the resulting masses of the stellar disc and of the DM halo, are similar. In fact, we have:

$M_d = 8.8 \times 10^8 M_\odot$; $r_0 = 10.7 kpc$; $\rho_0 = 3.7 \times 10^{-3} M_\odot/pc^3$; $M_{vir} = 1.0 \times 10^{11} M_\odot$.

While, by considering the stellar disc + the DM halo + gaseous disc, we have:

$M_d = 8.0 \times 10^8 M_\odot$; $r_0 = 10.7 kpc$; $\rho_0 = 3.2 \times 10^{-3} M_\odot/pc^3$; $M_{vir} = 8.2 \times 10^{10} M_\odot$; $M_{HI} = 1.0 \times 10^9 M_\odot$.

In the above, M_d, r_0, ρ_0, M_{HI} (the quantities obtained by fitting $V_{co-add}(x, V_{opt})$) are the stellar disc mass, the DM halo core radius, the central core mass density, the HI gaseous disc mass (including the correction for helium contribution), respectively. M_{vir} is the virial mass.

More importantly, we show in Fig. 8 that the difference in the crucial quantity f_b in the two different cases is small. There is only a slightly increase at outer galactic radii in the latter case: the resulting data move further towards the equality line ($g = g_b$), making our results stronger. See Fig. 9.

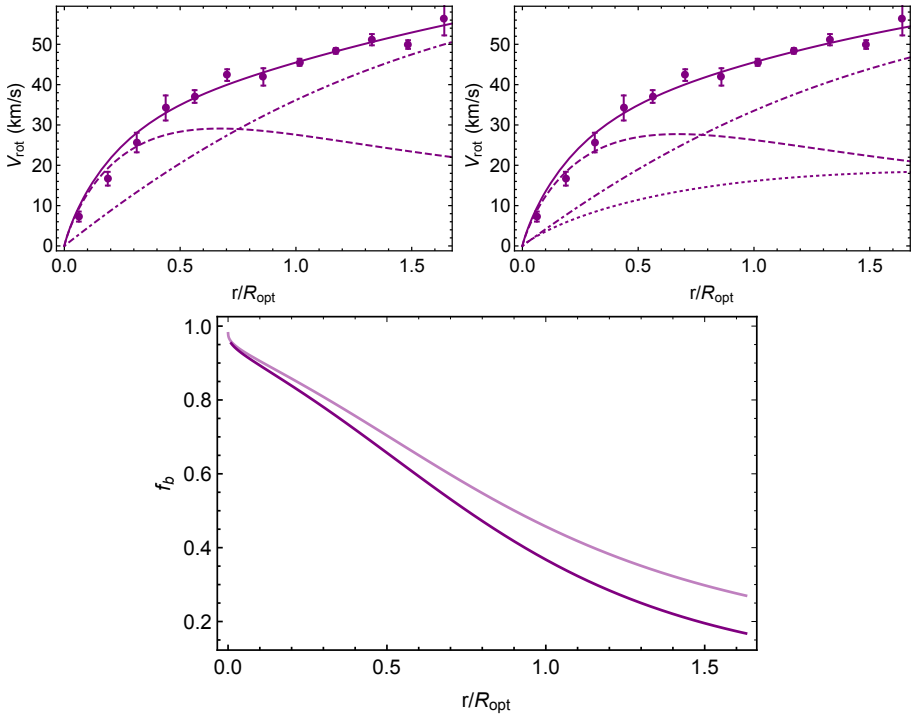


Figure C8:. *Upper panels*: I velocity bin (*family*) rotation curve fitted without and with gas. The *dashed, dot-dashed, dotted* and *solid lines* stand for the stellar disc, the DM halo, the gaseous disc and the total contributions to the rotation curve, respectively. *Bottom panel*: baryonic fraction without gas (*dark purple*) and with gas (*light purple*).

D. FITTING UNCERTAINTIES ON F_B: THE EFFECTS ON THE G - G_B PLANE

The error induced by the kinematical estimation of the stellar mass M_d is very small. Fig. 10 shows the results in the g - g_b plane, taking into account a $\pm 2\sigma$ fitting errors on f_b (which is the main source of error). The outcome doesn't change. See Fig. 10 and 1.

E. THE ANALYSIS OF THE G - X AND G - G_B RELATIONS IN INDIVIDUAL GALAXIES

It is easier to understand what happens in the g - g_b plane and in the g - g_b - x space by analysing a number of single galaxies. Fig. 11 shows the rotation curves, its fits, g vs r/R_{opt} relationship and g vs g_b relationship, for three LSBs of different size. The disagreement of present data with McG+16 relationship is evident galaxy by galaxy. Detailed explanation on this will appear on Di Paolo et al. (2018) in prep.

F. THE LSB SAMPLE

In Tab. 1, we report the list of LSB galaxies used in this work and the references of their rotation curves data and other galactic properties.

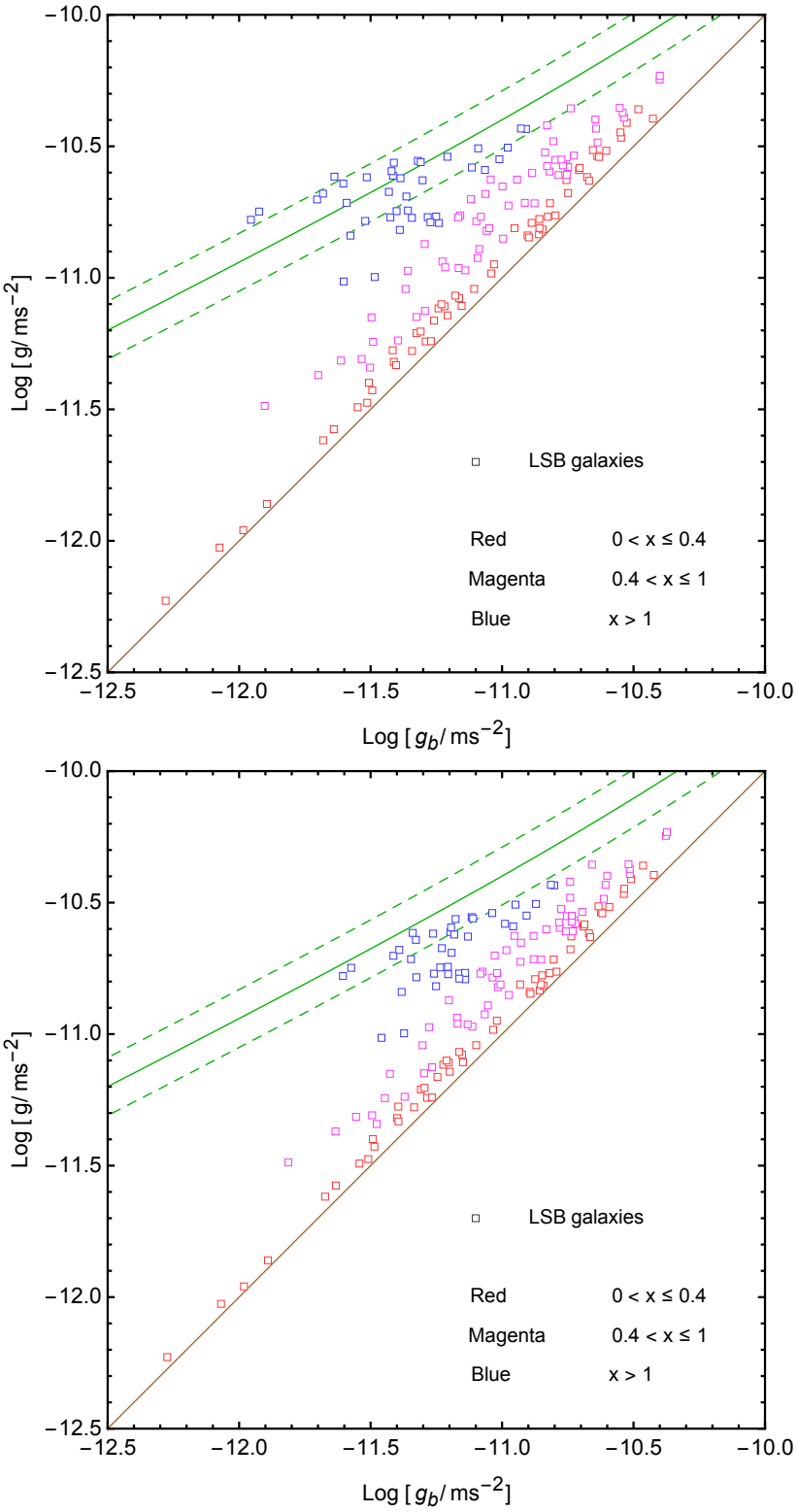


Figure C9:. Data resulting from galaxies belonging to the I velocity bin (*family*) rotation curve fitted without gas (*left panel*) and with gas (*right panel*).

REFERENCES

Burkert, A. 1995, ApJ, 447, L25

Das, M. 2013, Journal of Astrophysics and Astronomy, 34, 19

de Block, E. 2000, Encyclopedia of Astronomy and Astrophysics, doi:10.1888/0333750888/2620

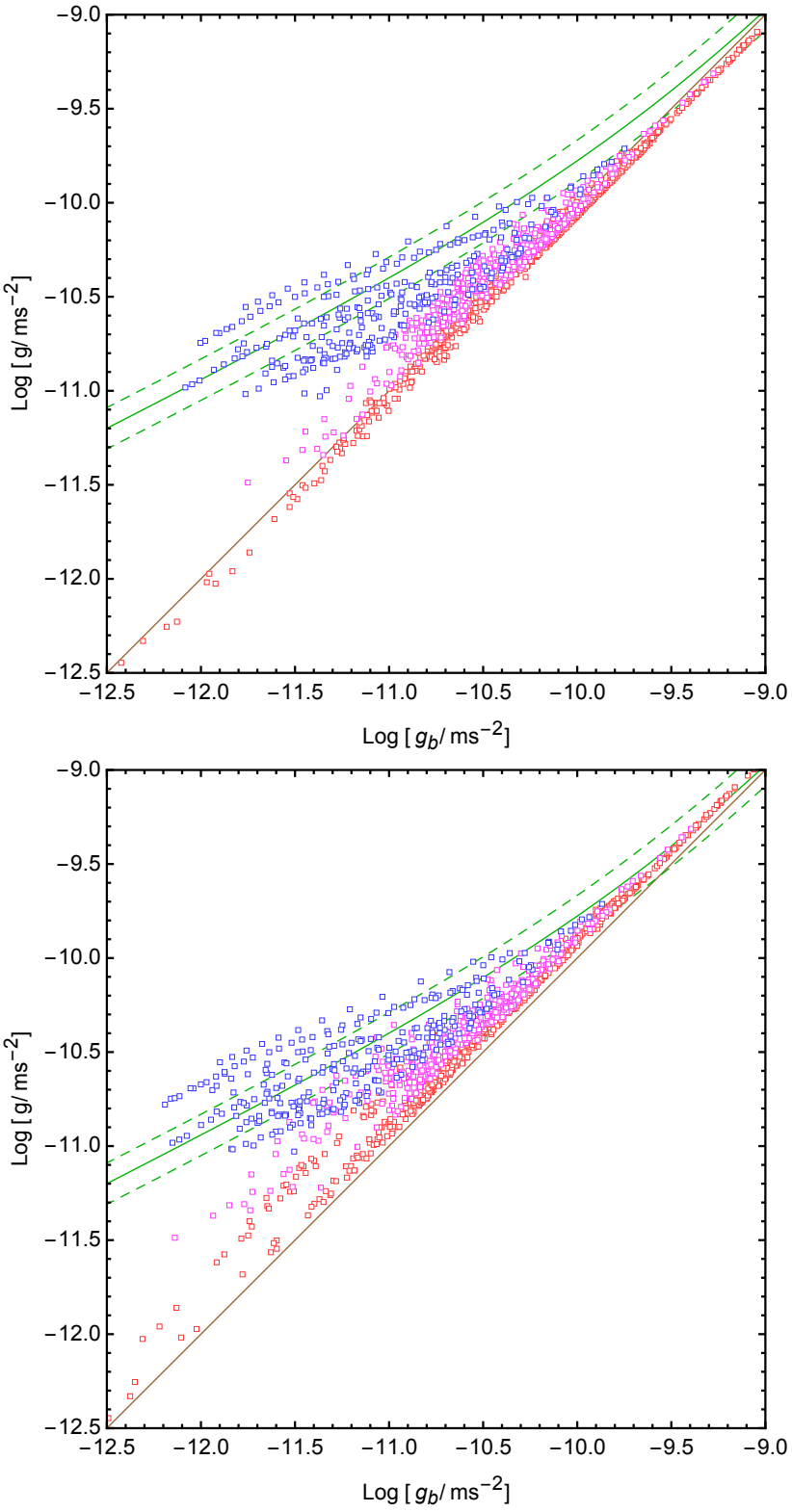


Figure D10:. The g - g_b relationship by assuming that f_b is 2σ higher (*left panel*) and 2σ lower than the best value (*right panel*).

de Blok, W. J. G., & Bosma, A. 2002, AandA, 385, 816

Di Paolo, C., & Salucci, P. 2018, arXiv:1805.07165v1

Evoli, C., Salucci, P., Lapi, A., & Danese, L. 2011, ApJ, 743, 45

Freeman, K. C. 1970, ApJ, 160, 811

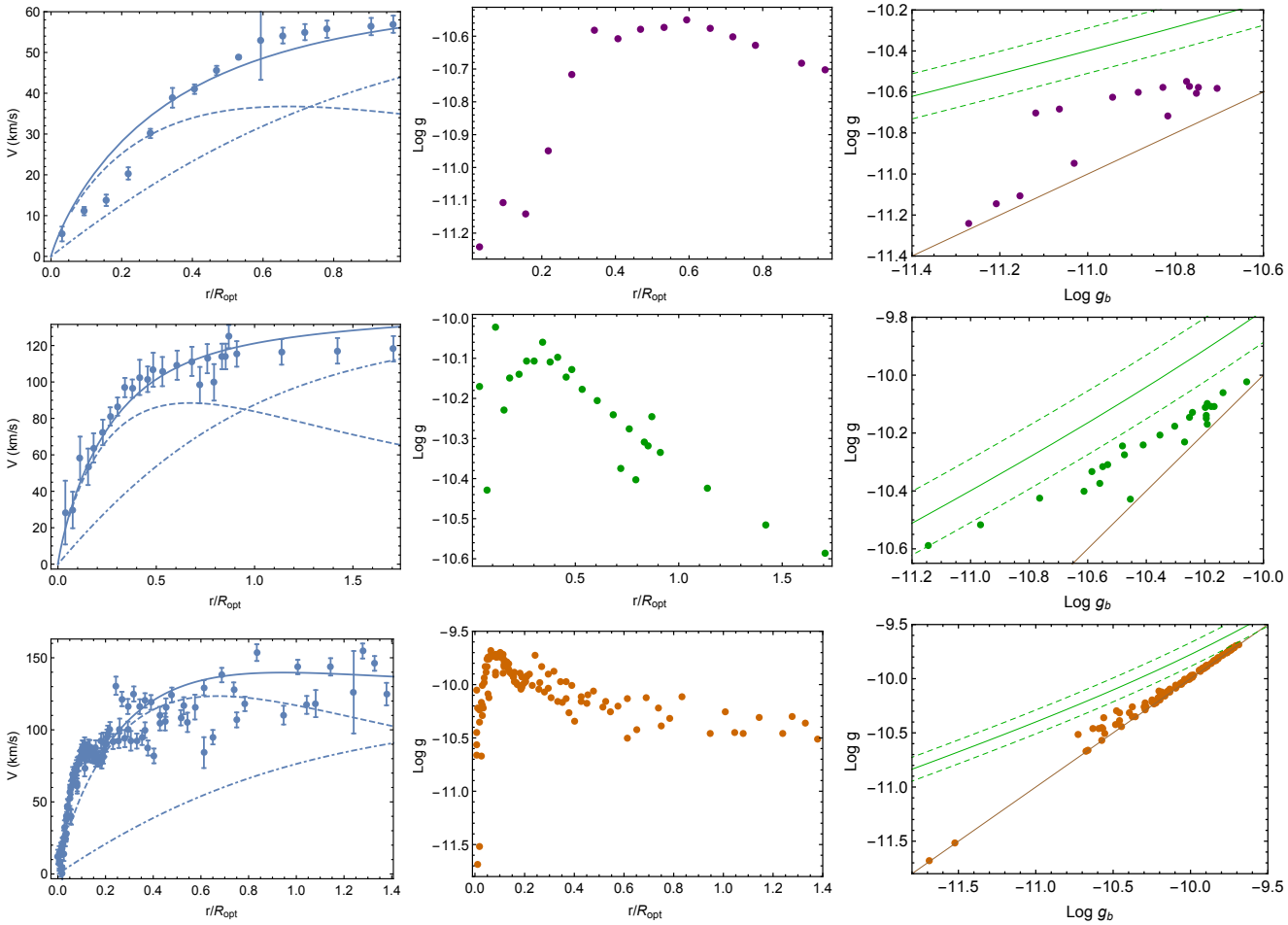


Figure E11:. The *first, second* and *third row* refers respectively to the galaxies: UGC1281, F568V1, ESO234-G013. Each row shows the galaxy's rotation curve with fit, g vs r/R_{opt} relationship and g vs g_b relationship. The *green* and the *brown lines* are the McGaugh relationship (with its 1σ uncertainties) and the equality $g = g_b$ relation, both independent on the radial coordinate r/R_{opt}.

Impey, S., & Bothun, G. 1997, Annu. Rev. Astron. Astrophys., 35, 267

Karachentsev, I. D., Makarov, D. I., & Kaisina, E. I. 2013, AJ, 145, 101

Karukes, E. V., & Salucci, P. 2017, MNRAS, 465, 4703

Lapi, A., Salucci, P., & Danese, L. 2018, Astrophysical Journal, 859, 19

Lelli, F., McGaugh, S. S., & Schombert, J. M. 2016, Astron. J, 152, 157

Li, P., Lelli, F., McGaugh, S., & Schombert, J. 2018, Astronomy and Astrophysics, 615, 70

McGaugh, S., Lelli, F., & Schombert, J. 2016, Phys. Rev. Lett., 117, 201101

McGaugh, S. S. 1994, Astrophysical Journal, 426, 135

Persic, M., & Salucci, P. 1991, ApJ, 368, 60

Persic, M., Salucci, P., & Stel, F. 1996, MNRAS, 281, 27

Salucci, P. 2018a, Foundation of Physics, 48, 1517

—. 2018b, arXiv:1807.08521. Proceedings of the 18th Lomonosov Conference on Elementary Particle Physics, edited by Alexander Studenikin, World Scientific (Singapore), 2018

Salucci, P., & Burkert, A. 2000, ApJ, 537, L9

Salucci, P., Lapi, A., Tonini, C., et al. 2007, MNRAS, 378, 41

Salucci, P., Ratnam, C., Monaco, P., & Danese, L. 2000, MNRAS, 317, 488

Tonini, C., Lapi, A., Shankar, F., & Salucci, P. 2006, ApJ, 638, L13

Wang, J., Fu, J., Aumer, M., et al. 2014, MNRAS, 441, 2159

Yegorova, I., & Salucci, P. 2007, MNRAS, 377, 507

Galaxy	M	Filter	R_d	V_{opt}	Reference
	mag		kpc	km/s	
(1)	(2)	(3)	(4)	(5)	(6)
NGC 100	-19.68	I	1.2	77.2	de Blok & Bosma, 2002
NGC 247	-18.01	B	2.9	106.6	Carignan & Puche, 1990
NGC 959	-18.53	V	0.93	75.3	Kuzio de Naray et al. 2008
NGC 2552	-18.99	I	1.6	104.9	Kuzio de Naray et al. 2008
NGC 2552	-18.99	I	1.6	111.0	de Blok & Bosma, 2002
NGC 2552	-18.99	I	1.6	92.6	Swaters et al. 2003
NGC 2552	-18.1	R	1.6	92.5	van den Bosch & Swaters, 2001
NGC 3274	-16.7	R	0.5	79.7	de Blok & Bosma, 2002
NGC 3274	-16.6	R	0.45	63.2	Swaters et al. 2003
NGC 3347B	-21.76	I	8.1	167.0	Palunas & Williams, 2000
NGC 4395	-18.1	R	2.3	82.0	de Blok & Bosma, 2002
NGC 4395	-18.14	R	2.6	82.6	van den Bosch & Swaters, 2001
NGC 4455	-16.9	R	0.7	45.6	de Blok & Bosma, 2002
NGC 4455	-16.88	R	0.9	61.9	Marchesini et al. 2002
NGC 4455	-16.88	R	0.9	51.5	van den Bosch & Swaters, 2001
NGC 5023	-19.18	I	0.8	78.4	de Blok & Bosma, 2002
NGC 5204	-17.3	R	0.66	75.2	Swaters et al. 2003
NGC 5204	-17.28	R	0.66	71.0	van den Bosch & Swaters, 2001
NGC 7589	-21.9	R	13	224.0	Pickering et al. 1997
UGC 628	-19.2	R	4.7	130.0	de Blok & Bosma, 2002
UGC 634	-17.7	B	3.1	95.1	van Zee et al. 1997
UGC 731	-16.6	R	1.7	73.1	de Blok & Bosma, 2002
UGC 731	-16.6	R	1.6	73.5	Swaters et al. 2003
UGC 731	-16.63	R	1.6	73.5	van den Bosch & Swaters, 2001
UGC 1230	-19.1	R	4.5	104.5	de Blok & Bosma, 2002
UGC 1230	-17.16	NUV	4.4	89.7	van der Hulst et al. 1993
UGC 1281	-16.2	R	1.7	45.8	Kuzio de Naray et al. 2006
UGC 1281	-16.2	R	1.7	56.9	de Blok & Bosma, 2002
UGC 1551	-19.7	B	2.5	55.8	Kuzio de Naray et al. 2008
UGC 2684	-13.7	B	0.8	36.7	van Zee et al. 1997
UGC 2936	-21.1	R	8.4	255.0	Pickering et al. 1999
UGC 3137	-18.7	R	2.0	97.7	de Blok & Bosma, 2002
UGC 3174	-15.7	B	1.0	51.7	van Zee et al. 1997
UGC 3371	-17.7	R	3.1	84.7	de Blok & Bosma, 2002
UGC 3371	-17.74	R	3.1	85.1	van den Bosch & Swaters, 2001
UGC 4115	-15.21	V	0.4	24.2	McGaugh et al. 2001
UGC 4278	-17.7	R	2.3	92.6	de Blok & Bosma, 2002
UGC 5005	-17.8	B	4.4	95.5	de Blok & McGaugh, 1997
UGC 5272	-14.7	B	1.2	51.2	Kuzio de Naray et al. 2008
UGC 5272	-14.7	B	1.2	46.4	de Blok & Bosma, 2002
UGC 5716	-16.3	B	2.0	66.4	van Zee et al. 1997
UGC 5750	-19.5	R	5.6	58.5	Kuzio de Naray et al. 2006
UGC 5750	-19.5	R	5.6	78.5	de Blok & Bosma, 2002
UGC 5999	-12.42	R	4.4	153.0	van der Hulst et al. 1993
UGC 7178	-16.6	B	2.3	69.9	van Zee et al. 1997
UGC 8837	-15.7	R	1.2	49.6	de Blok & Bosma, 2002
UGC 9211	-16.21	R	1.3	61.9	van den Bosch & Swaters, 2001
UGC 11454	-22.03	R	4.5	150.3	McGaugh et al. 2001
UGC 11557	-19.7	R	3.1	83.7	Swaters et al. 2003
UGC 11583	-15.48	R	0.31	27.9	McGaugh et al. 2001

Table F1:. LSB sample. Columns: (1) galaxy name; (2) magnitude, given for further information of the galaxies; (3) filter; (4) stellar disc scale length R_d; (5) optical velocity V_{opt}; (6) reference. Note that some galaxies have multiple rotation curve data, that we have homogenised.

Galaxy	M	Filter	R_d	V_{opt}	Reference
	mag		kpc	km/s	
(1)	(2)	(3)	(4)	(5)	(6)
UGC 11616	-21.58	R	4.9	133.2	McGaugh et al. 2001
UGC 11648	-22.95	KS	3.8	142.2	McGaugh et al. 2001
UGC 11748	-23.02	R	3.1	240.7	McGaugh et al. 2001
UGC 11819	-20.62	R	5.3	154.6	McGaugh et al. 2001
ESO 186-G055	-20.62	R	3.6	133.2	Pizzella et al., 2008
ESO 206-G014	-20.32	R	5.2	91.3	Pizzella et al. 2008
ESO 215-G039	-21.72	I	4.2	142.9	Palunas & Williams, 2000
ESO 234-G013	-21.66	I	3.7	139.4	Pizzella et al. 2008
ESO 268-G044	-21.19	I	1.9	175.6	Palunas & Williams, 2000
ESO 322-G019	-20.41	B	2.5	100.7	Palunas & Williams, 2000
ESO 323-G042	-21.56	I	4.4	138.7	Palunas & Williams, 2000
ESO 323-G073	-21.81	I	2.1	165.3	Palunas & Williams, 2000
ESO 374-G003	-21.36	I	4.2	118.3	Palunas & Williams, 2000
ESO 382-G006	-17.03	R	2.3	160.0	Palunas & Williams, 2000
ESO 400-G037	-20.96	I	4.1	69.9	Pizzella et al. 2008
ESO 444-G021	-19.9	B	6.4	107.4	Palunas & Williams, 2000
ESO 444-G047	-21.11	I	2.7	148.4	Palunas & Williams, 2000
ESO 488-G049	-17.94	B	4.4	95.3	Pizzella et al. 2008
ESO 509-G091	-21.01	I	3.7	146.8	Palunas & Williams, 2000
ESO 534-G020	-21.96	R	17	216.6	Pizzella et al. 2008
F561-1	-17.8	B	3.6	50.8	de Blok et al. 1996
F563-V1	-16.3	B	2.4	27.3	de Blok et al. 1996
F563-V2	-18.2	B	2.1	98.8	Kuzio de Naray et al. 2006
F563-V2	-17.6	B	2.1	98.0	de Blok et al. 1996
F565-V2	-14.8	B	2.0	45.2	de Blok et al. 1996
F568-1	-18.1	B	5.3	130.1	Swaters et al. 2000
F568-3	-19.14	I	4.0	102.6	Kuzio de Naray et al. 2006
F568-3	-18.3	B	4.0	97.9	McGaugh et al. 2001
F568-3	-18.3	B	4.0	101.1	Swaters et al. 2000
F568-6	-23.6	R	18	297.0	Pickering et al. 1997
F568-V1	-17.9	B	3.2	115.8	Swaters et al. 2000
F571-8	-17.6	B	5.2	139.4	Marchesini et al. 2002
F571-8	-17.6	B	5.2	140.1	McGaugh et al. 2001
F571-V1	-11.47	I	3.2	72.44	de Blok et al. 1996
F574-1	-18.4	B	4.3	102.3	Swaters et al. 2000
F574-2	-17	B	4.5	40.0	de Blok et al. 1996
F579-V1	-18.8	B	5.1	111.5	McGaugh et al. 2001
F583-1	-16.5	B	1.6	68.2	Kuzio de Naray et al. 2008
F583-1	-17.06	R	1.6	65.2	Marchesini et al. 2002
F583-1	-16.5	B	1.6	61.3	McGaugh et al. 2001
F583-1	-15.9	B	1.6	53.3	de Blok et al. 1996
F583-4	-16.9	B	2.7	83.9	Kuzio de Naray et al. 2006
F583-4	-16.9	B	2.7	69.0	McGaugh et al. 2001
F730-V1	-20.27	R	5.8	141.6	McGaugh et al. 2001
PGC 37759	-21.88	Z	6.6	139.4	Morelli et al. 2012

Table F2:. It continues from Tab. 1.